Postprint of: Science of the Total Environment 605-606: 147-157 (2017)

Assessing the effects of UVA photocatalysis on soot-coated TiO_2-containing mortars

José María de la Rosa[1], Ana Z. Miller[1*], J. Santiago Pozo-Antonio[2,3], José Antonio González-Pérez[1], Nicasio T. Jiménez-Morillo[1], Amelia Dionisio[3]

[1] Instituto de Recursos Naturales y Agrobiología de Sevilla, Consejo superior de Investigaciones Científicas (IRNAS-CSIC). Avenida Reina Mercedes 10, 41012, Sevilla, Spain.

[2] Departamento de Enxeñaría de Recursos Naturais e Medioambiente, Escola de Minas, Universidade de Vigo, Campus Lagoas-Marcosende, 36310 Vigo, Spain.

[3] CERENA, Instituto Superior Técnico, Universidade de Lisboa. Av. Rovisco Pais, 1049-001 Lisboa, Portugal.

***Corresponding author:**

A.Z. Miller (anamiller@irnas.csic.es)

Abstract

The deposition of soot on building surfaces darkens their colour and leads to undesirable black crusts, which are one of the most serious problems on the conservation of built cultural heritage. As a preventive strategy, self-cleaning systems based on the use of titanium dioxide (TiO_2) coatings have been employed on building materials for degrading organic compounds deposited on building surfaces, improving their durability and performance. In this study, the

self-cleaning effect of TiO_2-containing mortars coated with diesel soot has been appraised under laboratory conditions. The mortar samples were manufactured using lime putty and two different doses of TiO_2 (2.5% and 5%). The lime mortars were then coated with diesel engine soot and irradiated with ultraviolet A (UVA) illumination for 30 days. The photocatalytic efficiency was evaluated by visual inspection, field emission scanning electron microscopy (FESEM) and colour spectrophotometry. Changes in the chemical composition of the soot particles (including persistent organic pollutants) were assessed by analytical pyrolysis (Py-GC/MS) and solid state ^{13}C NMR spectroscopy.

The FESEM and colour spectrophotometry revealed that the soot-coated TiO_2-containing mortars promoted a self-cleaning effect after UVA irradiation. The combination of analytical pyrolysis and ^{13}C solid state NMR showed that the UVA irradiation caused the cracking of polycyclic aromatic structures and *n*-alkyl compounds of the diesel soot and its transformation into methyl polymers. Our findings also revealed that the inclusion of TiO_2 in the lime mortar formulations catalysed these transformations promoting the self-cleaning of the soot-stained mortars. The combined action of TiO_2 and UVA irradiation is a promising proxy to clean lime mortars affected by soot deposition.

Keywords: UVA irradiation; diesel soot; TiO_2; analytical pyrolysis; lime-based mortar; cultural heritage conservation.

INTRODUCTION

In urban environments, the deposition of air pollutants and organic particulate matter (soot particles, polycyclic aromatic hydrocarbons, sulphur compounds, spores) is responsible for the formation of black crusts on building envelope surfaces (Hermosin et al., 2004; Montana et al., 2008; Papida et al., 2000). Nowadays, these crusts represent one of the most important deterioration forms on the European built heritage with significant aesthetic, economic and cultural implications (ICOMOS, 2008; Pozo-Antonio et al., 2016; Rivas et al., 2014; Sleiman et al., 2014, 2015). This has prompted the seeking of novel engineering and conservation strategies to reduce soot deposition on cultural heritage assets (Karatasios et al., 2010; Ruot et al., 2009).

Soot particles are produced during incomplete combustion processes, such as car engines, industries, domestic heating systems or forest fires, from volatile precursor compounds formed during pyrolysis that subsequently release carbon-rich particles (Schmidt and Noack, 2000). This pyrogenic organic material is omnipresent in the atmosphere, soils, sediments, ice and building surfaces due to its widespread emission in most industrial cities and high stability in the environment (Goldberg, 1985). Other persistent organic pollutants are the polycyclic aromatic hydrocarbons (PAHs), which are occluded in the soot matrix during the incomplete combustion process (De la Rosa et al., 2016). Despite soot particles were traditionally considered relatively unreactive, this pyrogenic organic matter can indeed be degraded (De la Rosa and Knicker, 2011). Kim et al. (2013) showed that soot-associated PAHs can be degraded by photolysis. Energetic UV photons have sufficient energy to disrupt chemical bonds in many materials including soot particles. The absorption of UV energy

can cause the breaking and/or crosslinking of polymeric compounds, leading to altered chemical and mechanical properties of the polymers. After disruption of the initial chemical state, the polymers are likely to react with oxygen and/or water vapour causing additional changes. Another type of photo-degradation can occur due to photo-absorption by inorganic pigment particles such as titanium dioxide (TiO_2). An electron–hole pair is formed in the pigment particle. A photo-excited hole can then migrate to the particle's surface and cause a deleterious chemical reaction in the polymer (Kim et al., 2013). For this reason, white TiO_2 nanoparticles are usually tested as thin coatings on building surfaces to mitigate biological colonization and fuel soot deposition on mortars (Bengtsson and Castollete, 2014; Diamanti et al., 2008; Fonseca et al., 2010; Munafò et al., 2015; Paolini et al., 2016; Pinho et al., 2013; Quagliarini et al., 2012; Senff et al.,2013; Smits et al., 2013). Anatase is one of the most common crystalline forms of TiO_2 and is characterized by its great photocatalysis, which is the acceleration of a photochemical reaction by means of a catalyst interacting with light of sufficient energy (Lucas et al., 2013; Toma et al., 2004). The photocatalytic reaction takes place on the surface of the building materials where the adsorption of the gaseous pollutants occurs (Fujishima et al., 2008). Despite carbon photo-oxidation has been previously reported (Kim et al., 2013), the chemical changes experimented by soot-derived organic compounds are not well understood.

This study assessed the photocatalytic degradation of diesel soot particles deposited on lime-based mortars containing TiO_2 nanoparticles after 30 days of UVA irradiation. For these purposes, visual examination, field emission scanning electron microscopy (FESEM), colour spectrophotometry, Solid State

^{13}C Nuclear Magnetic Resonance (NMR) Spectroscopy and Pyrolysis coupled with Gas Chromatography/Mass Spectrometry (analytical pyrolysis) were applied.

Several authors have determined the photocatalytic action of TiO_2 particles by colorimetry and SEM (Pinho et al., 2013; Smits et al., 2013). Nevertheless and to the best of our knowledge, this is the first study combining solid-state ^{13}C NMR and analytical pyrolysis for assessing the effects of UVA irradiation and TiO_2 on the composition of diesel soot particles deposited on lime-based mortars. Moreover, there are no previous studies in the literature using real diesel soot deposits collected from combustion engines to test the photocatalytic action of TiO_2 on building materials under laboratory conditions.

Analytical pyrolysis is a powerful tool widely used for the direct characterisation of organic mixtures with diverse origin which, owing to their complexity, are difficult to analyse by both conventional destructive or non-destructive methods (Gonzalez-Perez et al., 2014). In fact it has become a valuable tool for the characterisation of complex carbonaceous matrices, including soot and urban dust on building surfaces (De la Rosa et al., 2008; Pereira de Oliveira et al., 2011). The solid-state ^{13}C NMR has been widely used in the characterization of refractory organic matter forms in soils and sediments and more recently has been successfully applied to study the composition of pyrogenic carbon, including soot and other forms of black carbon (De la Rosa et al., 2008; De la Rosa and Knicker, 2011).

2. MATERIALS AND METHODS

2.1. Sample preparation

In this work, lime-based mortars were prepared with different concentrations of TiO_2 and coated with diesel engine exhaust soot. These soot particles were collected from diesel automobile pipes in Lisbon city centre (Portugal) using a smooth brushing.

The binder used for preparing the mortar samples was a commercial 5-year packaged lime putty with a bulk density of 1.35 kg dm^{-3}. As provided by the supplier (C.T.S., Getafe, Spain), its chemical composition is: CaO (88.0-90.0%), MgO (0.0-0.5%), SiO_2+Al_2O_3+Fe_2O_3 (0.1-0.3%), and CO_2 (2.5-3.5%). In addition, a 45±5% of water was added to the mix. The mineralogical composition of this lime putty is portlandite [$Ca(OH)_2$] (86.0-88.0 %) and calcite [$CaCO_3$] (7.0-9.0 %). The aggregate used was a commercial siliceous sand (0.08/2.00 mm particles) with a bulk density of 2.60 kg dm^{-3} supplied by BIC *Materiales y Conservación* (Pontevedra, Spain), in accordance with the requirements of the Standard Specification for Concrete Aggregates ASTM C33 (2013).

The photocatalytic additive added to the mortar samples was a commercial titanium dioxide product (P-25) from Degussa AG (Frankfurt, Germany), consisting of predominantly nanocrystalline anatase with a specific surface area of 50 m^2 g^{-1}, a bulk density of 0.13 kg dm^{-3} and a particle size of approximately 20 nm.

Three mortar formulations with different concentration of TiO_2 (0, 2.5 and 5 wt.% with respect to the total solid content) were prepared (Table 1). For each formulation, three mortar samples of 6 cm x 6 cm x 2 cm were manufactured as

described in Lucas et al. (2013) and Pozo-Antonio (2015). Samples were prepared with a lime/aggregate ratio of 1/3 (by weight). The components were mixed manually, without any previous treatment, using a laboratory blender. The water/binder ratio was fixed at 0.45. The fresh mortars were cast into acrylic moulds and maintained during one month under laboratory conditions (20±5ºC and 60±10% RH) covered with sackcloth and a black plastic. During this period, the samples were sprayed with distilled water every day to obtain high hydration avoiding carbonation. After demoulding, the lime mortar samples were cured during one month under laboratory conditions (18±5ºC and 60±10% RH) to promote the transformation of portlandite into calcite (carbonation), a fundamental process for making mortars harder (Cultrone et al., 2005). The mortar samples were covered with sackcloth and a black plastic to avoid interaction with light during mortar curing. Physical and mechanical properties of these lime-based mortars are described in Pozo-Antonio and Dionisio (2017).

An average amount of 8 mg cm^{-2} of diesel soot was applied with a brush on the surface of each sample. Twenty four hours later, the soot-coated surface of each sample was sprayed with ~5 ml of deionised water and brushed with a soft-bristled scrub to remove the excess of diesel soot and ensure the contact between soot and TiO_2-containing mortar surfaces. This procedure resulted in a heterogeneous soot layer of maximum 3 µm in thickness on each mortar surface. The samples were dried for one week at room temperature and protected from light, as mentioned above. Subsequently, the mortar samples were submitted to UVA irradiation (315 nm < λ < 400 nm) in a closed custom-made box during 30 days (720 hours), following Smits et al. (2013). The UVA irradiation was performed using three Philips Special TL-D 18 W lamps, which

were placed at 2.5 cm above the samples. The mean UV light flux onto the sample surfaces, measured with a ELSEC 764 Environmental Monitor (Dorset, United Kingdom), was 8.63 W m^{-2}. It is slightly higher than the 6.11 W m^{-2} irradiance tested by Shen et al. (2012) and registered in a cloudy fall day in Pullman, Washington (Shen et al., 2012).

2.2. Assessment of photocatalytic oxidation of diesel soot particles

2.2.1 Field emission scanning electron microscopy

The photocatalytic soot oxidation was firstly evaluated by naked-eye visualisation. A more detailed examination was performed by field emission scanning electron microscopy (FESEM), using a Jeol JSM-7001F microscope equipped with an Oxford X-ray energy dispersive spectroscopy (EDS) detector, to analyse each mortar formulation before soot application, to measure the soot thickness and to detect soot remains on the surface after 30 days under UVA irradiation. In addition, the morphology and chemical composition of the diesel soot samples before application onto the mortar surfaces were assessed by FESEM-EDS. FESEM examinations were operated in both secondary electron (SE) and Back Scattered Electrons (BSE) detection modes on samples previously coated with a thin gold-palladium film.

2.2.2 Colour spectrophotometry

For characterising the colour of the manufactured mortars, the CIELAB colour parameters (CIE S014-4/E:2007) were measured using a Minolta portable spectrophotometer (model CM-508i). A total of 15 random measurements were obtained from the upper surface of each mortar sample for the three replicates

of each mortar formulation before soot deposition (0 days of UVA irradiation), and after 30 days of UVA irradiation. The three CIELAB colour parameters were measured: L* (lightness), which varies from 0 (black) to 100 (white); a*, which is related to colour changes in the red–green range (+a*: red and -a*: green); and b*, associated with changes in yellow–blue range (+b*: yellow and -b*: blue). The measurements of the L*, a* and b* parameters were taken in specular component included (SCI) mode, for a spot diameter of 8 mm with diffuse illumination by means of xenon flash arc lamp and 10 nm diffuse bandwidth, using illuminant D65 at observer angle 2° (ASTM-D2244, 2014). The CIELAB colour differences (ΔL*, Δa* and Δb*) were calculated considering the colour of the pure lime mortar before soot deposition as reference, corresponding to the cleanest surface. Thus, variations in the three colour parameters were calculated as follows:

$\Delta L^* = L^*_f - L^*_0$;

$\Delta a^* = a^*_f - a^*_0$;

$\Delta b^* = b^*_f - b^*_0$;

where L^*_f, a^*_f, b^*_f is the mean value of the CIELAB colour parameter after 30 days of UVA irradiation, and L^*_0, a^*_0, b^*_0 is the mean value of the CIELAB colour parameter before soot deposition. The total colour difference (ΔE^*_{ab}) were calculated as follows (CIE S014-4/E:2007): $\Delta E^*_{ab} = [(\Delta L^*)^2 + (\Delta a^*)^2 + (\Delta b^*)^2]^{1/2}$

2.2.3 Pyrolysis-Gas Chromatography Mass Spectrometry (Py-GC/MS)

Direct pyrolysis-gas chromatography/mass spectrometry (Py-GC/MS) was performed using a double-shot pyrolyser (Frontier Laboratories, model 2020i)

attached to a GC/MS Agilent 6890N system. Each sample (1-2 mg) was placed in a small crucible capsule and introduced into a preheated micro-furnace at 500°C for 1 min. The volatile pyrolysates were then directly injected into the GC/MS for analysis. The gas chromatograph was equipped with a HP-5ms-UI, low polar-fused silica (5%-Phenyl-methylpolysiloxane) capillary column of 30 m × 250 μm × 0.25 μm film thickness. The oven temperature was held at 50°C for 1 min and then increased to 100°C at 30°C min^{-1}, from 100°C to 300°C at 10°C min^{-1}, and stabilized at 300°C for 10 min. The carrier gas was helium at a controlled flow of 1 ml min^{-1}. The detector consisted of an Agilent 5973 mass selective detector, and mass spectra were acquired at 70 eV ionizing energy. Compound assignment was achieved by taking advantage of: i) ion chromatography via single-ion monitoring (SIM) for the major various homologous series, ii) via low-resolution mass spectrometry, and iii) via comparison with published data reported in the literature or stored in digital libraries (NIST and Wiley libraries). Every sample was pyrolyzed twice.

2.2.4. Solid-state ^{13}C NMR spectroscopy

Each sample (200-300 mg) for solid-state ^{13}C NMR spectroscopy was grounded in an agate mortar prior to analysis. The solid-state ^{13}C NMR spectra were obtained using a Bruker Avance III HD 400 MHz instrument operating at a frequency of 100.64 MHz and using ZrO_2 rotors of 4 mm OD for ^{13}C with Kel-F caps. The cross polarization (CP) technique was used during magic-angle spinning (MAS) of the rotor at 14 kHz for ^{13}C. The solid state ^{13}C NMR spectra were acquired using a ramped 1H-pulse during the 1 ms contact time to circumvent Hartmann-Hahn mismatches. Employing a pulse delay of 300 ms,

between 50,000 and 200,000 scans were accumulated. A line broadening of 150 Hz was used. The ^{13}C chemical shifts were calibrated relative to tetramethylsilane (0 ppm) with glycine (COOH at 176.08 ppm). The spectra were quantified by subdividing them into the following chemical shift regions as described in Knicker (2011): alkyl C (0–45 ppm); *N*-alkyl/methoxyl C (45–60 ppm); *O*-alkyl C (60–110 ppm); aromatic C (110–160 ppm); carbonyl/amide C (160–250 ppm). The ^{13}C intensity distribution was determined by integrating signal intensity over the above-mentioned chemical shift regions using the MestreNova 10 software (Santiago de Compostela, Spain). The soot-coated mortar without TiO_2 (before and after UVA irradiation) was used as control to compare its direct soot photodegradation with the TiO_2-UVA photocatalytic oxidation.

3. RESULTS AND DISCUSSION

3.1. Macro and microscopic observations

On the basis of the visual evaluation, the mortar samples after curing and before soot application exhibited white-coloured surfaces with apparent high porosity and roughness (sample L0, Fig. 1A). After soot deposition and brushing (to remove the excess of diesel soot and ensure the contact between soot and TiO_2 nanoparticles), the mortar surfaces exhibited a thin and heterogeneous dark grey coating, darker on areas where soot penetrated deeply into the mortar pores (sample SL0, Fig. 1B). This inevitable heterogeneity of the thin soot layer due to the mortar texture was also reported in the literature (e.g. Chin et al., 2009; Simts et al., 2013). After 30 days of UVA irradiation, the diesel soot-

stained mortar without TiO_2 (SL0+UVA, Fig. 1C) showed no visual differences when compared with the soot-coated mortar before UVA exposure (SL0, Fig. 1B). In contrast, the surface of the soot-coated mortars containing 2.5% (SL2.5+UVA, Fig. 1D) and 5% (SL5+UVA, Fig. 1E) of TiO_2 turned into light grey after UVA exposure. They exhibited whiter surfaces than before UVA irradiation, but not their original white-coloured surface before soot deposition (Fig. 1A). Dark soot staining was still visible on the mortar pores (Fig. 1D,E). This suggests that the diesel soot film was greatly oxidized but not completely, probably due to the texture of the mortar samples.

FESEM-EDS analyses of the bulk soot samples before their application onto the mortar surfaces revealed aggregates of very small (< 50 nm) carbonaceous particles rich almost exclusively in C (Fig. 2A and EDS spectrum 1). These aggregates greatly varied in size, ranging from 2 µm to 15 µm, and depict very porous structures. The carbon-rich aggregates were also observed containing P, S, Ca and Fe (Fig. 2A,B and corresponding EDS spectra). Their morphology and chemical composition are characteristic of diesel soot (Uy et al., 2014).

FESEM images of the lime-based mortars revealed the characteristic mineralogical phases obtained due to the carbonation process of lime mortars (Rodriguez-Navarro et al., 2007; Cizer et al., 2012). In the lime-based mortar without TiO_2, both plate-like crystals of portlandite and micrometre-sized calcite rhombohedra crystals were identified (Fig. 3A). In samples with TiO_2 the precipitation of scalenohedral calcite crystals with a rosette-like shape were abundant on the outer surface (Fig. 3B,C), corresponding to the carbonation layer. These calcite crystals grow from the surface of plate-like portlandite

crystals as observed in Figure 3C. Such morphology results from the full transformation of portlandite into calcite after carbonation in air for 60 days (Cizer et al., 2012). Aggregations of TiO_2 nanoparticles added during the mortar manufacturing process were observed on the mortar surfaces, even within the carbonation layer as observed in Figure 3C and corresponding EDS spectrum.

Concerning the lime-based mortars after soot deposition and UVA irradiation, FESEM-EDS analyses revealed that soot particles with their characteristic morphology and composition rich in C were present on the mortar surfaces with 0% TiO_2 (Fig. 3D,E). In contrast, the soot layer on the surface of the mortar samples with 2.5% and 5% of TiO_2 (Fig. 3F and 3G, respectively) almost disappear, evidencing an effective soot decomposition. A photocatalytic degradation study by Lee and Choi (2002) reported that a *n*-hexane soot layer (~2 µm thickness) on TiO_2 films deposited on glass plates was completely oxidised after more than 30h of UV irradiation as revealed by SEM. They observed that the soot oxidation occurred both at the soot/TiO_2 interface and in the bulk of the soot layer. As reported, photooxidants (particularly OH radicals) generated on the TiO_2 film migrated into the bulk of the porous soot layer, indicating that the amount of soot in direct contact with the TiO_2 film is independent of the soot thickness (Lee and Choi, 2002).

3.2. Colour spectrophotometry

Colorimetric measurements were performed for the lime-based mortars containing TiO_2 before and after soot deposition, and after 30 days under UVA irradiation. Table 2 shows the colorimetric differences (ΔL^*, Δa^*, Δb^* and ΔE^*_{ab}) for the soot-coated mortar without TiO_2 (SL0) and the samples with 2.5%

(SL2.5) and 5% (SL5) of TiO_2 after UVA irradiation using as reference the colour of the pure lime mortar before soot deposition. Hence, the lower the difference, the better the self-cleaning effect.

The coordinate L* was the main responsible for the total colour difference (ΔE^*_{ab}), showing a decrease of 14 CIELAB units for samples containing TiO_2. This evidences the efficiency of the TiO_2 catalyst for degrading the diesel soot layer. However, the values of parameters a* and b* increased in relation to the colour of the mortar without TiO_2 due to the increase of yellowish and brownish tones associated with soot degradation. Diamanti et al. (2008) considered the variation of the chromatic coordinates L* and b* as representative of dirt accumulation on a surface. Also, Sanmartín et al. (2012) demonstrated that the parameter b* is the most useful for early detecting the darkening of granite surfaces by phototrophic colonization. Indeed and according to Diamanti et al. (2008, 2013), the mineralization of organic compounds formerly adsorbed on the surface can be the cause of the colour changes of the surface to more yellow hues. Considering the CIELAB colour wheel, the soot-coated mortar surfaces after UVA exposure showed browner hues (CIE S014-4/E:2007) than before soot deposition. This is consistent with the visual inspection (Fig. 1), and indicates that a complete photocatalytic oxidation of the soot particles was not achieved. The values of the total colour differences (Fig. 4) were much higher (>30 CIELAB units) than the threshold established for an unexperienced observer ($\Delta E^* \leq 2$, Mokrzycki and Tatol, 2012) and higher than the threshold acceptable in Conservation of Cultural Heritage ($\Delta E^* \leq 5$, García and Malaga, 2012). Comparing both samples containing TiO_2, the mean value of the total colour difference for the lime-mortar with the highest TiO_2 content was slightly

lower (ΔE^*_{ab} = 29.70, Fig. 4) than the value obtained for the mortar with 2.5% TiO_2 (ΔE^*_{ab} = 30.25, Fig. 4). This indicates that the darkening on the mortar surface with 5% TiO_2 slightly decreased.

The colour spectrophotometry findings reported in this study are contradictory to those obtained by Smits et al. (2013). These authors observed a complete photocatalytic oxidation of a carbon black pigment on mortars coated with TiO_2, obtaining total colour differences less than 5 CIELAB units, which is the threshold acceptable in Conservation of Cultural Heritage (Munafò et al. 2015). However, it is important to note that: i) the authors used an artificial soot composed of 0.1% carbon black in 8:2 water:isopropanol solution, while in the current approach, real diesel soot matter from car pipes was used, and ii) Smits et al. (2013) applied TiO_2 films over mortar surfaces, while TiO_2 was added during the mortar manufacturing process performed in this study. Hence, the procedures and parameters used should be taken into account for making comparisons. In fact, the works reviewed by Munafò et al. (Munafò et al. 2015 and references therein), shared the application of artificial dyes (e.g. methyl red, rhodamine B, methylene blue and methyl orange) to stain the samples before UVA exposure, instead of real diesel soot particles. They also differed in the quantity of dye, the intensity of UVA irradiation, its wavelength range and the total time of exposure to UV light.

3.3 Chemical changes occurred during photocatalytic soot oxidation

The chemical changes of the organic matter occurred during the photocatalytic oxidation of the soot particles deposited on the lime mortars were evaluated using Py-GC/MS and ^{13}C Solid-State NMR Spectroscopy.

3.3.1 Analytical pyrolysis (Py-GC/MS)

The total ion chromatogram (TIC) and a list of the released compounds obtained by GC/MS analysis of the pyrolysates generated at 500ºC are reported in Figure 5 and Table 3, respectively. Clear differences were found when comparing the pyrochromatograms of the bulk soot (Fig. 5A) and soot-coated mortars before UVA irradiation (Fig. 5B,C) with the soot-coated mortars after UVA exposure (Fig. 5D-F). The pyrochromatogram of the pure lime mortar (Fig. 5G) was used for comparison purposes as the cleanest possible sample. The scarcity of pyrolysis-releasing organic compounds (volatiles) from the pure mortar material is evident in Figure 5G. Its TIC showed small peaks corresponding to benzene, toluene, styrene and benzonitrile (see peaks 1, 3, 8 and 13 respectively in Table 3). Moldoveanu (2010) and Pereira de Oliveira et al., (2011) reported that benzene (peak 1), toluene (3), phenol, benzonitrile (13) and naphthalene were produced in the pyrolysis of 5-amino-isophthalic acid. Thus, they are probably derived from the pyrolysis of polyamides usually present in lime mortars as dispersant additive for easier mixing and application. No proteinaceous or lipid material were detected in the pure lime mortar. Their contents are probably below the limit of detection, which is very common in lime mortars (Rampazzi et al., 2016).

Figure 5A-C shows the TIC of the bulk soot sample, soot-coated mortar without TiO_2 (SL0) and soot-coated mortar with 5% TiO_2 (SL5) before UVA irradiation. These pyrochromatograms are quite similar due to the scarcity of pyrolysis-releasing organic compounds from the lime mortar substrate. They are dominated by aromatic compounds derived from benzene (toluene, methyl-

benzenes, etc), and polycyclic aromatic hydrocarbons (PAHs), being naphthalenes, biphenyls and phenanthrene the most abundant (peaks 23, 28, 31, 32, 45 and 47 in Fig. 5A,B and Table 3). The PAHs are the result of combustion-generated airborne particulate matter. Pyrogenic PAHs are suggested to be partially occluded in the soot matrix (during the incomplete combustion process), due to their extremely high affinities to the aromatic flat surfaces of soot (Eganhouse, 1997; Readman et al., 1984). They have been identified, among other sources, in smoke particles and diesel or gasoline engine soot (Yu and Hites, 1981). Their high relative abundance may indicate a great condensation degree of the studied soot samples. A homologous series of *n*-alkanes and *n*-alkenes, ranging from C_9 (1-Nonene; peak 7) to C_{33} (tritriacontane; peak 71), added to a few fatty acids (C_{16}, C_{18} and C_{30} fatty acid methyl esters; see peaks 52, 57 and 72) were also detected. They are petroleum residues and predominant components of lipids from aerosols in urban environments (Simoneit, 1986). These compounds have been previously detected by Py-GC/MS in carbon deposited on historic building façades (Pereira de Oliveira et al., 2011; Saiz-Jimenez, 1992). The lack of diterpenoids in the pyrolysates indicates the absence of organic particles from wood combustion into the soot. The presence of TiO_2 in the non-irradiated sample (SL5, Fig. 5C) caused no visible alterations in comparison with the SL0 sample (Fig. 5B), excepting the lack of a few long-chain *n*-alkanes (peaks 66-70; Table 3). In contrast, after UVA irradiation a remarkable reduction of the pyrolysable material was observed (Fig. 5D-F). The pyrochromatogram of sample SL0 after UVA exposure (Fig. 5D) was still dominated by aromatic compounds and PAHs. Nevertheless, the relative abundance of highly condensed PAHs (3 or more

rings; see peaks 47, 53-56) decreased. The ratio of the relative abundance naphthalene:benzene (ratio of peaks 23:1) can be used as a sign of the cracking of PAHs. This ratio sharply decreased for the soot-coated mortars exposed to UVA, and the presence of TiO_2 enhanced this trend. Other remarkable difference caused by UVA exposure is the absence of long chain *n*-alkanes/enes and fatty acids in the soot-coated samples (Fig. 5D-F). Figure 5E and 5F shows the TICs of the soot-coated mortars with TiO_2 (doses of 2.5% and 5%, respectively) after UVA irradiation. Their TICs illustrate a drastic decrease of pyrolysable compounds, indicating that the presence of TiO_2 caused the removal of most of PAHs and alkyl compounds. In fact, these TICs are almost similar to the pure mortar pyrochromatogram (Fig. 5G), with the exception of the presence of naphthalene and biphenyl (peaks 23 and 28). The increase in the content of TiO_2 (from 2.5% to 5%) has not induced further changes as assessed by Py-GC/MS.

3.3.2 Solid state ^{13}C NMR spectroscopy

To confirm the results obtained by analytical pyrolysis, solid-state ^{13}C NMR spectroscopy was performed. This technique has been widely used in the characterization of soot present in black carbon-rich samples isolated from complex matrices such as soils and sediments (De la Rosa et al., 2008). The CP-MAS ^{13}C NMR spectra of the bulk soot, pure lime mortar and soot-coated samples are displayed in Figure 6. Table 4 shows the corresponding integration of the signals for each C region.

The ^{13}C NMR spectrum of the bulk soot (Fig. 6A) was performed to be able to distinguish between the ^{13}C signals derived from the soot and from the

pure lime mortar material (L0) in the soot-coated mortars. The spectrum of bulk soot (Fig. 6A) is dominated by a prominent peak at 128.3 ppm typically assigned to unsubstituted and alkyl substituted aromatic carbon (Wilson, 1987), which accounted for 49.8% of the total ^{13}C-intensity (Table 4), followed by signals of alkyl C (21.1 and 28.9 ppm and 15.6% of the total ^{13}C intensity) and a couple of bands at 153.3 and 163.9 ppm in the region corresponding to phenolic groups. The small signal at 196.1 ppm could indicate the presence of ketonic C-double bonds; nevertheless this signal is overestimated due to the contribution of spinning side bands (marked with an asterisk). Similarly to analytical pyrolysis, the ^{13}C NMR spectrum of the pure lime mortar should be taken as background, i.e., as reference for the best self-cleaning effect that can be achieved (soot-free sample). Therefore, the closer the spectra of the soot-coated samples are to the pure lime mortar, the more effective is the decomposition of soot. In fact, the ^{13}C NMR spectrum of the soot-coated mortar without TiO_2 and before UVA illumination (SL0, Fig. 6B) shows abundant changes in comparison with the bulk soot (Fig. 6A). Soot compounds are diluted in the mortar matrix and thus a combination of C-signals from the soot and mortar are observed in the ^{13}C NMR spectrum (Fig. 6B, control). The major peaks are present in the alkyl C region (31 and 39 ppm; 22.9% of the total ^{13}C intensity), at 65-67 and 71.7 ppm (alkyl-O carbon; from 23.9%), at 128 ppm (aromatic carbon; 30.0%) and at 167.9 ppm (carboxylic carbon; 8.8%).

Comparing the ^{13}C NMR spectra of the soot-coated mortar without TiO_2 (SL0) before (Fig. 6B) and after (Fig. 6C) UVA irradiation, few differences were observed. There was a slight decrease in the aromaticity of the soot-coated mortar after exposure to UVA (Fig. 6C) when compared with the non-irradiated

sample without TiO_2 (Fig. 6B). The % of aryl C decreased from 30.0 to 28.8% (Table 4). Concomitantly, the presence of alkyl C increased in the same order of magnitude after UVA irradiation. These alterations in the relative abundances of certain functional groups enhanced in the presence of TiO_2 for the UVA exposed soot-coated samples (SL2.5 and SL5, Table 4). In fact, the % of aryl C of the soot-coated mortar with 5% of TiO_2 (Fig. 6E) reached the same % of aryl C (24%) as the pure lime mortar (see SL5 and L0 in Table 4). This indicates that the aromatic fraction corresponding to the soot present on the mortar surface with 5% TiO_2 was completely degraded. Concomitantly with the reduction of aryl C (110-160 ppm), the relative contribution of O-alkyl C increased in the UVA-irradiated samples. Another interesting difference concerns the signal appearing at 29-31 ppm, which corresponds to CH_2 from alkyl chains. This peak is missing in samples with TiO_2 (Fig. 6D,E) which is in agreement with the breaking of alkyl structures reported by Py-GC/MS for these samples. The combined action of TiO_2/UVA also caused the disappearance of the small peaks at 153-154 ppm corresponding to phenols. The signals in the range 35-43 ppm are typically assigned to alkyl C in chain methylene structures (Knicker, 2000). They are also visible in the pure lime mortar due to the presence of methyl polymers.

4. Conclusions

This study revealed that TiO_2 catalysed the photodegradation of the diesel soot layer deposited on lime-based mortars containing TiO_2. Macroscopic observations, FESEM-EDS and colour spectrophotometry evidenced colour changes and the decomposition of soot on the surface of the soot-stained

mortars caused by the exposure of TiO_2 to UVA irradiation during 30 days. The analytical pyrolysis and solid state ^{13}C NMR spectroscopy showed evident alterations on the molecular composition of soot after UVA irradiation, which promoted the breaking of highly condensed polycyclic aromatic compounds and long chain *n*-alkyl homologues. This approach revealed that TiO_2 acted as catalytic agent enhancing the decomposition of the soot layer. This study demonstrated that the irradiation with UVA and the inclusion of TiO_2 in building materials is a promising preventive action to protect architectural cultural heritage assets affected by soot deposition.

ACKNOWLEDGEMENTS.

J.M. de la Rosa and A.Z. Miller thank The Spanish Ministry of Economy and Competitiveness (MINECO) for the “Ramón y Cajal” and Juan de la Cierva postdoctoral contracts, respectively. J.S. Pozo-Antonio was supported by a postdoctoral contract with the University of Vigo within the framework of the 2011–2015 Galician Plan for Research. Innovation and Growth (Plan I2C) for 2014. This work was also co-funded by the Strategic project FCT-UID/ECI/04028/2013.

References

ASTM-C33, 2013. Standard Specification for Concrete Aggregates.

ASTM-D2244, 2014 Standard Practice for Calculation of Color Tolerances and Color Differences from Instrumentally Measured Color Coordinates.

Bengtsson N., Castellote M., 2014. Heterogeneous photocatalysis on construction materials: effect of catalyst properties on the efficiency for degrading NOx and self cleaning. Materiales de Construcción 64, 314. DOI:10.3989/mc.2014.06713.

Chin P., Grant C.S., Ollis D.F., 2009. Quantitative photocatalyzed soot oxidation on titanium dioxide. Appl.Catal.B. 87, 220–229. DOI: 10.1016/j.apcatb.2008.09.020

CIE S014-4/E:2007, Colorimetry Part 4: CIE 1976 L*A*b* Colour Space, Commission Internationale de l'eclairage, CIE Central Bureau, Vienna, 2007.

Cizer O., Rodríguez-Navarro C., Ruiz-Agudo E., Elsen J., Van Gemert D., Van Balen K., 2012. Phase and morphology evolution of calcium carbonate precipitated by carbonation of hydrated lime. J. Mater. Sci. 47, 6151-6165. DOI: 10.1007/s10853-012-6535-7

Cohen J. D., Sierra-Gallego G., Tobón J.I., 2015. Evaluation of Photocatalytic Properties of Portland Cement Blended with Titanium Oxynitride (TiO2−xNy) Nanoparticles. Coatings 5, 465-476. DOI: 10.3390/coatings5030465

Cultrone G., Sebastián E., Ortega Huertas M., 2005. Forced and natural carbonation of lime-based mortars with and without additives: Mineralogical and textural changes. Cement Concrete Res. 35, 2278-2289. DOI:10.1016/j.cemconres.2004.12.012

De la Rosa J.M., Knicker H., 2011. Bioavailability of N released from N-rich pyrogenic organic matter: An incubation study. Soil Biol. Biochem. 43, 2368-2373. DOI: 10.1016/j.soilbio.2011.08.008

De la Rosa J.M., Gonzalez-Perez J.A., Hatcher P.G., Knicker H., Gonzalez-Vila F.J., 2008. Determination of refractory organic matter in marine sediments by chemical oxidation, analytical pyrolysis and solid-state ^{13}C nuclear magnetic resonance spectroscopy. Eur. J. Soil Sci. Soc. 59, 430–438. DOI: 10.1111/j.1365-2389.2007.00979.x

De la Rosa J.M., Paneque P., Hilber I., Blum F., Knicker H., Bucheli T.D., 2016. Assessment of polycyclic aromatic hydrocarbons in biochar and biochar amended agricultural soils from southern Spain. J. Soils Seds. 16, 557-565. DOI: 10.1007/s11368-015-1250-z

Diamanti M.V., Ormellese M., Pedeferri M.P., 2008. Characterization of photocatalytic and superhydrophilic properties of mortars containing titanium dioxide. Cem. Concr. Res. 38, 1349–1353. DOI: 10.1016/j.cemconres.2008.07.003

Diamanti M.V., Del Curto B., Ormellese M., Pedeferri M.P., 2013. Photocatalytic and self-cleaning activity of colored mortars containing TiO_2. Constr. Build. Mater. 46, 167-174. DOI: 10.1016/j.conbuildmat.2013.04.038

Eganhouse R.P., 1997. Eganhouse (Ed.), Molecular Markers in Environmental Geochemistry, American Chemical Society, Washington, DC. pp. 1–20

Fonseca A.J., Pina F., Macedo M.F., Leal N., Romanowska-Deskins A., Laiz L., Gómez-Bolea A., Saiz-Jimenez C., 2010. Anatase as an alternative application for preventing biodeterioration of mortars: Evaluation and comparison with other biocides. Int. Biodeter. Biodegr. 64, 388-396. DOI: 10.1016/j.ibiod.2010.04.006

Fujishima A., Zhang X.T., Tryk D.A., 2008. TiO_2 photocatalysis and related surface phenomena. Surf. Sci. Rep. 63, 515–582. DOI: 10.1016/j.surfrep.2008.10.001

García O., Malaga K., 2012. Definition of the procedure to determine the suitability and durability of an anti-graffiti product for application on cultural heritage porous materials. J. Cult. Herit. 13, 77-82. DOI: 10.1016/j.culher.2011.07.004

Goldberg E.D., 1985. Black Carbon in the Environment. Wiley-Interscience, N.Y.

González-Pérez J.A., Almendros G., de la Rosa J.M., González-Vila F.J., 2014. Appraisal of polycyclic aromatic hydrocarbons (PAHs) in environmental matrices by analytical pyrolysis (Py–GC/MS). J. Anal. Appl. Pyrolysis 109, 1-8. DOI: 10.1016/j.jaap.2014.07.005

Hermosin B., Gaviño M., Saiz-Jimenez C., 2004. Organic compounds in black crusts from different European monuments: a comparative study. In: Saiz-Jimenez, C. (ed.) Air Pollution and Cultural Heritage. A. A. Balkema, Rotterdam, 47-55.

ICOMOS, “Illustrated glossary on stone deterioration patterns”, ICOMOS International Scientific Committee for Stone, 2008 (ISBN: 978-2-918086-00-0).

Karatasios I., Katsiotis M. S., Likodimos V., Kontos A. I., Papavassiliou G., Falaras P., Kilikoglou V., 2010. Photo-induced carbonation of lime-TiO2 mortars. Appl. Catal., B 95, 78–86. DOI: 10.1016/j.apcatb.2009.12.011

Kim D., Ypung T.M., Anastasio C., 2013. Phototransformation rate constants of PAHs associated with soot particles. Sci. Total Environ. 443, 896-903. DOI: 10.1016/j.scitotenv.2012.11.055

Knicker H., 2000. Biogenic nitrogen in soils as revealed by solid-state 13C and 15N NMR spectroscopy. J. Env. Qual. 29, 715-723. DOI: 10.2134/jeq2000.00472425002900030005x

Knicker H., 2011. Solid state CPMAS ^{13}C and ^{15}N NMR spectroscopy in organic geochemistry and how spin dynamics can either aggravate or improve spectra interpretation. Org. Geochem. 42, 867-890. DOI: 10.1016/j.orggeochem.2011.06.019

Lee M.C., Choi W., 2002. Solid phase photocatalytic reaction on the soot/TiO_2 interface: The role of migrating OH radicals. J. Phys. Chem. B 106, 11818-11822. DOI: 10.1021/jp026617f

Lucas S.S., Ferreira V.M., Barroso de Aguiar J.L., 2013. Incorporation of titanium dioxide nanoparticles in mortars — Influence of microstructure in the hardened state properties and photocatalytic activity. Cem. Concr. Res. 43, 112–120. DOI: 10.1016/j.cemconres.2012.09.007

Mokrzycki W.S., Tatol M., 2012. Colour difference ΔE - A survey. Machine Graphics and Vision. 20, 383-411.

Moldoveanu S.C., 2010. Pyrolysis of Organic Molecules with Applications to Health and Environmental Issues. In: Serban C. Moldoveanu (ed.) Techniques and Instrumentation in Analytical Chemistry. Elsevier, Volume 28, pp. 1-724. DOI: 10.1016/S0167-9244(09)02830-3

Montana G., Randazzo L., Oddo I.A., Valenza M., 2008. The growth of ‘‘black crusts’’ on calcareous building stones in Palermo (Sicily): a first appraisal of anthropogenic

and natural sulphur sources. Environ. Geol. 56, 367–380. DOI: 10.1007/s00254-007-1175-y

Munafò P., Goffredo G., Quagliarini E., 2015. TiO_2-based nanocoatings for preserving architectural stone surfaces: An overview. Constr. Build. Mater. 84, 201–218. DOI: 10.1016/j.conbuildmat.2015.02.083

Papida S., Murphy W., May E., 2000. Enhancement of physical weathering of building stones by microbial populations. Int. Biodeter. Biodegr 46, 305-317. DOI: 10.1016/S0964-8305(00)00102-5

Pereira de Oliveira B., De la Rosa J.M., Miller A.Z., Saiz-Jimenez C., Gómez-Bolea A., Sequeira Braga M.A., Dionísio A., 2011. An integrated approach to assess the origins of black films on a granite monument. Environ. Earth Sci. 63, 1677–1690. DOI: 10.1007/s12665-010-0773-2

Paolini R., Sleiman M., Pedeferri M., Diamanti M.V., 2016. TiO_2 alterations with natural aging: Unveiling the role of nitric acid on NIR reflectance, Sol. Energ. Mat. Sol. C. 157, 791-797. DOI: 10.1016/j.solmat.2016.07.052

Pinho L., Elhaddad F., Facio D.S., Mosquera M.J., 2013. A novel TiO_2–SiO_2 nanocomposite converts a very friable stone into a self-cleaning building material. Appl. Surf. Sci. 275, 389– 396. DOI: 10.1016/j.apsusc.2012.10.142

Pozo-Antonio J.S., 2015. Evolution of mechanical properties and drying shrinkage in lime-based and lime cement-based mortars with pure limestone aggregate. Constr. Build. Mater. 77, 472–478. DOI: 10.1016/j.conbuildmat.2014.12.115

Pozo-Antonio J.S., Rivas T., Fiorucci M.P., Ramil A., López A.J., 2016. Effectiveness of granite cleaning procedures in cultural heritage: a review. Sci. Total Environ. 571, 1017–1028. DOI: 10.1016/j.scitotenv.2016.07.090

Pozo-Antonio J.S., Dionisio A., 2017. Physical-mechanical properties of mortars with addition of TiO_2 nanoparticles. Constr. Build. Mater. 148, 261-272. DOI: 10.1016/j.conbuildmat.2017.05.040

Quagliarini E., Bondioli F., Battista Goffredo G., Cordoni C., Munafò P., 2012. Self-cleaning and de-polluting stone surfaces: TiO_2 nanoparticles for limestone. Constr. Build. Mater. 37, 51–57. DOI: 10.1016/j.conbuildmat.2012.07.006

Rampazzi L., Colombini M.P., Conti C., Corti C., Lluveras-Tenorio A., Sansonetti A., Zanaboni M. 2016. Technology of Medieval Mortars: An Investigation into the Use of Organic Additives. Archaeometry 58, 115-130. DOI: 10.1111/arcm.12155

Readman J.W., Mantoura R.F., Rhead M.M., 1984. The physico-chemical speciation of polycyclic aromatic hydrocarbons (PAH) in aquatic systems. Fresenius Z Anal Chem. 319, 126–131. DOI: 10.1007/BF00584673

Rivas T., Pozo S., Paz M., 2014. Sulphur and oxygen isotope analysis to identify sources of sulphur in gypsum-rich black crusts developed on granites. Sci. Total Environ. 482-483, 137-147. DOI: 10.1016/j.scitotenv.2014.02.128

Rodriguez-Navarro C., Jimenez-Lopez C., Rodriguez-Navarro A., Gonzalez-Muñoz M.T., Rodriguez-Gallego M., 2007. Complex biomineralized vaterite structures encapsulating bacterial cells. Geochim. Cosmochim. Acta. 71, 1197-1213. DOI: 10.1016/j.gca.2006.11.031

Ruot B., Plassais A., Olive F., Guillot L., Bonafous L., 2009. TiO_2-containing cement pastes and mortars: Measurements of the photocatalytic efficiency using a rhodamine B-based colourimetric test. Solar Energy. 83, 1794-1801. DOI: 10.1016/j.solener.2009.05.017

Saiz-Jimenez C., 1992. Deposition of airborne organic pollutants on historical buildings. Atmos. Environ. 278, 77-85. DOI: 10.1016/0957-1272(93)90047-A

Sanmartín P., Vázquez-Nion D., Silva B., Prieto B., 2012. Spectrophotometric color measurement for early detection and monitoring of greening on granite buildings. Biofouling 28, 329-338. DOI: 10.1080/08927014.2012.673220

Schmidt M.W.I., Noack A., 2000. Black carbon in soils and sediments: analysis, distribution, implications, and current challenges. Glob. Biog. Cycles. 14, 777–793. DOI: 10.1029/1999GB001208

Senff L., Tobaldi D.M., Lucas S., Hotza D., Ferreira V.M., Labrincha J.A., 2013. Formulation of mortars with nano-SiO_2 and nano-TiO_2 for degradation of pollutants in buildings. Composites: Part B. 44, 40–47. DOI: 10.1016/j.compositesb.2012.07.022

Shen S., Burton M., Jobson B., Haselbach L., 2012. Pervious concrete with titanium dioxide as a photocatalyst compound for a greener urban road environment. Constr. Build. Mater. 35, 874–883. DOI: 10.1016/j.conbuildmat.2012.04.097

Simoneit B.R.T., 1986. Characterization of Organic Constituents in Aerosols in Relation to Their origin and Transport: A Review. Int. J. Environ. Anal. Chem. 23, 207-237. DOI: 10.1080/03067318608076446

Sleiman M., Kirchstetter T.W., Berdahl P., Gilbert H.E., Quelen S., Marlot L., Preble C.V., Chen S., Montalbano A., Rosseler O., Akbari H., Levinson R., Destaillats H., 2014. Soiling of building envelope surfaces and its effect on solar reflectance – Part II: Development of an accelerated aging method for roofing materials. Sol. Energ. Mat. Sol. C. 122, 271-281. DOI: 10.1016/j.solmat.2013.11.028

Sleiman M., Chen S., Gilbert H.E., Kirchstetter T.W., Berdahl P. et al., 2015. Soiling of building envelope surfaces and its effect on solar reflectance – Part III: Interlaboratory study of an accelerated aging method for roofing materials. Sol. Energ. Mat. Sol. C. 143, 581-590. DOI: 10.1016/j.solmat.2015.07.031

Smits M., kit Chan C., Tytgat T., Craeye B., Costarramone N., Lacombe S., Lenaerts S., 2013. Photocatalytic degradation of soot deposition: Self-cleaning effect on titanium dioxide coated cementitious materials. Chem. Eng. J. 222, 411–418. DOI: 10.1016/j.cej.2013.02.089

Toma F.L., Bertrand G., Klein D., Coddet C., 2004. Photocatalytic removal of nitrogen oxides via titanium dioxide. Environ. Chem. Lett. 2, 117–121. DOI: 10.1007/s10311-004-0087-2

Uy D., Ford M.A., Jayne D.T., O'Neill A.E., Haack L.P., Hangas J., Jagner M.J., Sammut A., Gangopadhyay A.K., 2014. Characterization of gasoline soot and

comparison to diesel soot: Morphology, chemistry, and wear. Tribol. Int. 80, 198–209. DOI: 10.1016/j.triboint.2014.06.009

Wilson, M.A., 1987. NMR Techniques and Applications in Geochemistry and Soil Chemistry. Pergamon, Oxford.

Yu, M. L., Hites, R. A., 1981. Identification of organic compounds on diesel engine soot. Anal. Chem. 53, 951 -954. DOI: 10.1021/ac00230a005

Figures:

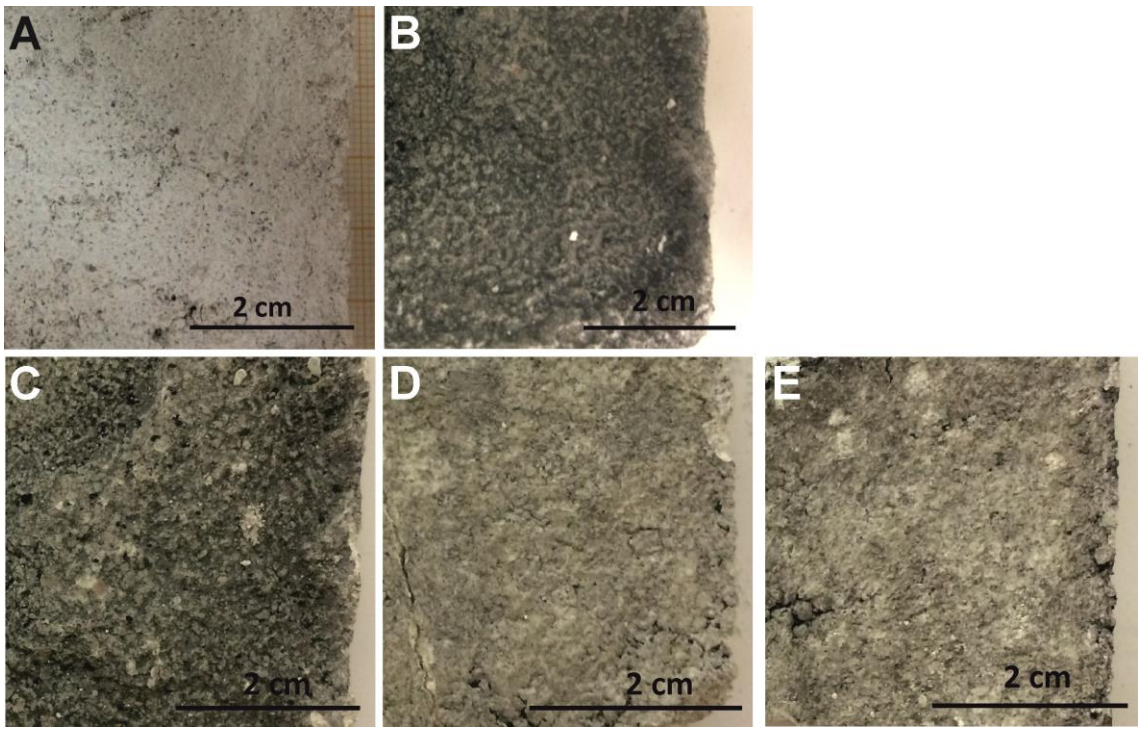

Figure 1. Digital photographs of lime-based mortars: A) Before soot deposition; B) after soot deposition and before UVA irradiation; C) with0% TiO_2 after UVA irradiation; D) 2.5%TiO_2 after UVA irradiation, and E) with 5% TiO_2 after UVA irradiation.

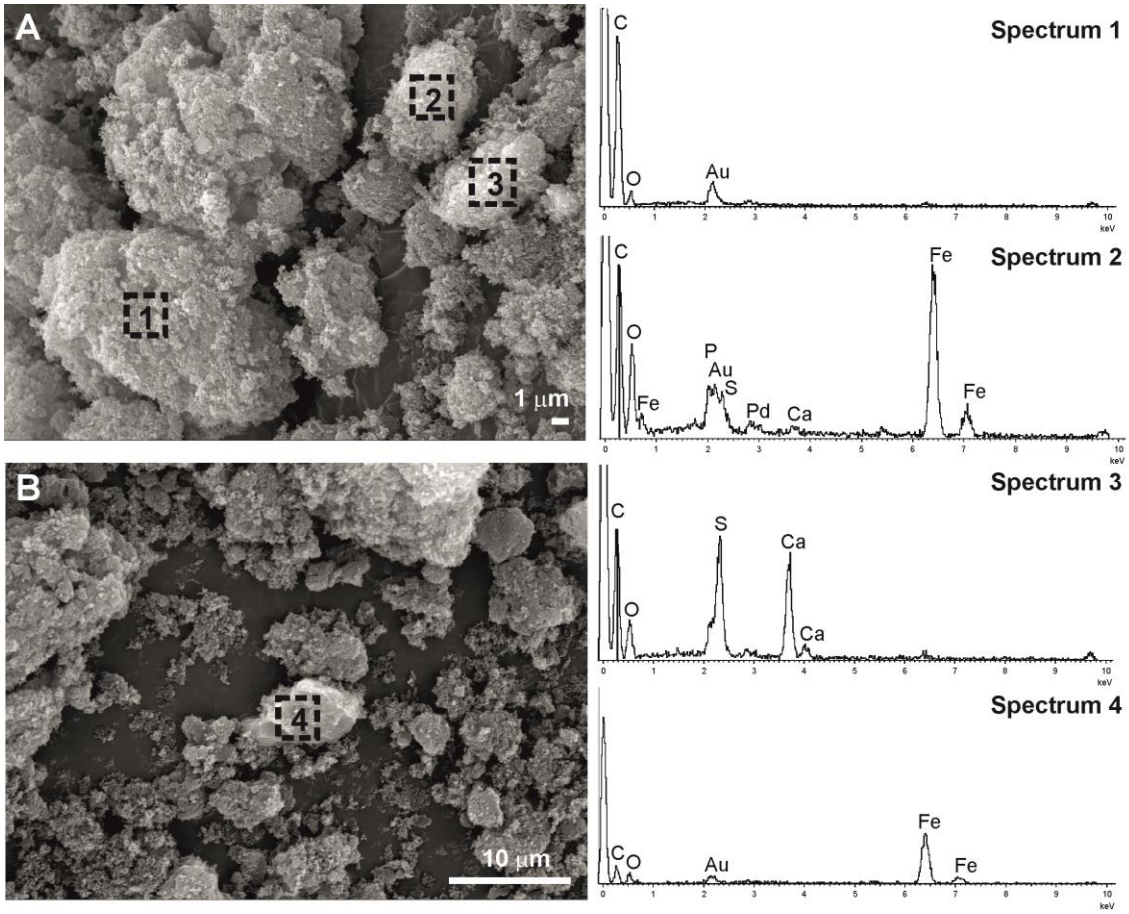

Figure 2. FESEM images of the bulk diesel soot samples before application onto mortar surfaces. A) Soot porous aggregates rich in C and P, S, Ca and Fe, and EDS spectra recorded in positions 1, 2 and 3. B) Fe-rich particle associated with soot and corresponding EDS spectrum recorded in position 4.

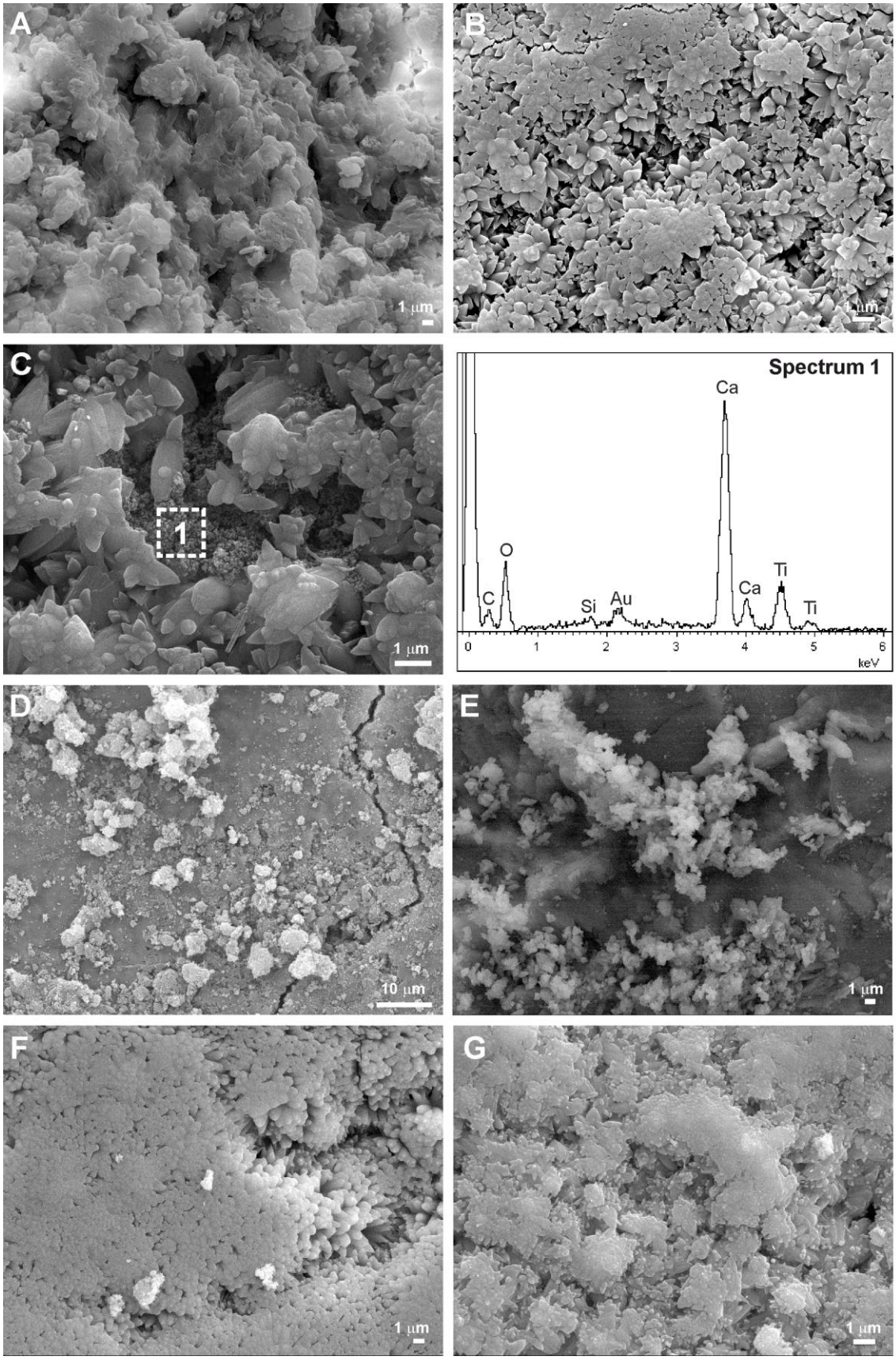

Figure 3. FESEM images of the lime-based mortars used in this study: A) lime mortar with 0% TiO_2 before soot deposition (L0); B) lime mortar with 2.5%TiO_2

before soot deposition (L2.5); C) lime mortar with 5%TiO_2 before soot deposition and corresponding EDS spectrum; D) soot-coated mortar with 0% TiO_2 after UVA irradiation (SL0+UVA); E) close-up view of soot particles on sample SL0+UVA; F) soot-coated mortar with 2.5%TiO_2 after UVA irradiation (SL2.5+UVA), and G) soot-coated mortar with 5%TiO_2 after UVA irradiation (SL5+UVA).

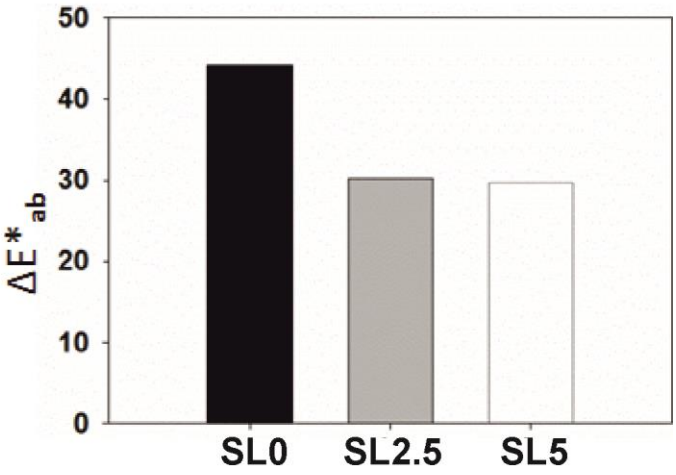

Figure 4. Total colour differences (ΔE^*_{ab}) of the soot-coated mortars with 0% (SL0), 2.5% (SL2.5) and 5% (SL5) TiO_2 after 30 days under UVA irradiation using as reference the initial colour of the pure lime mortar before diesel soot deposition.

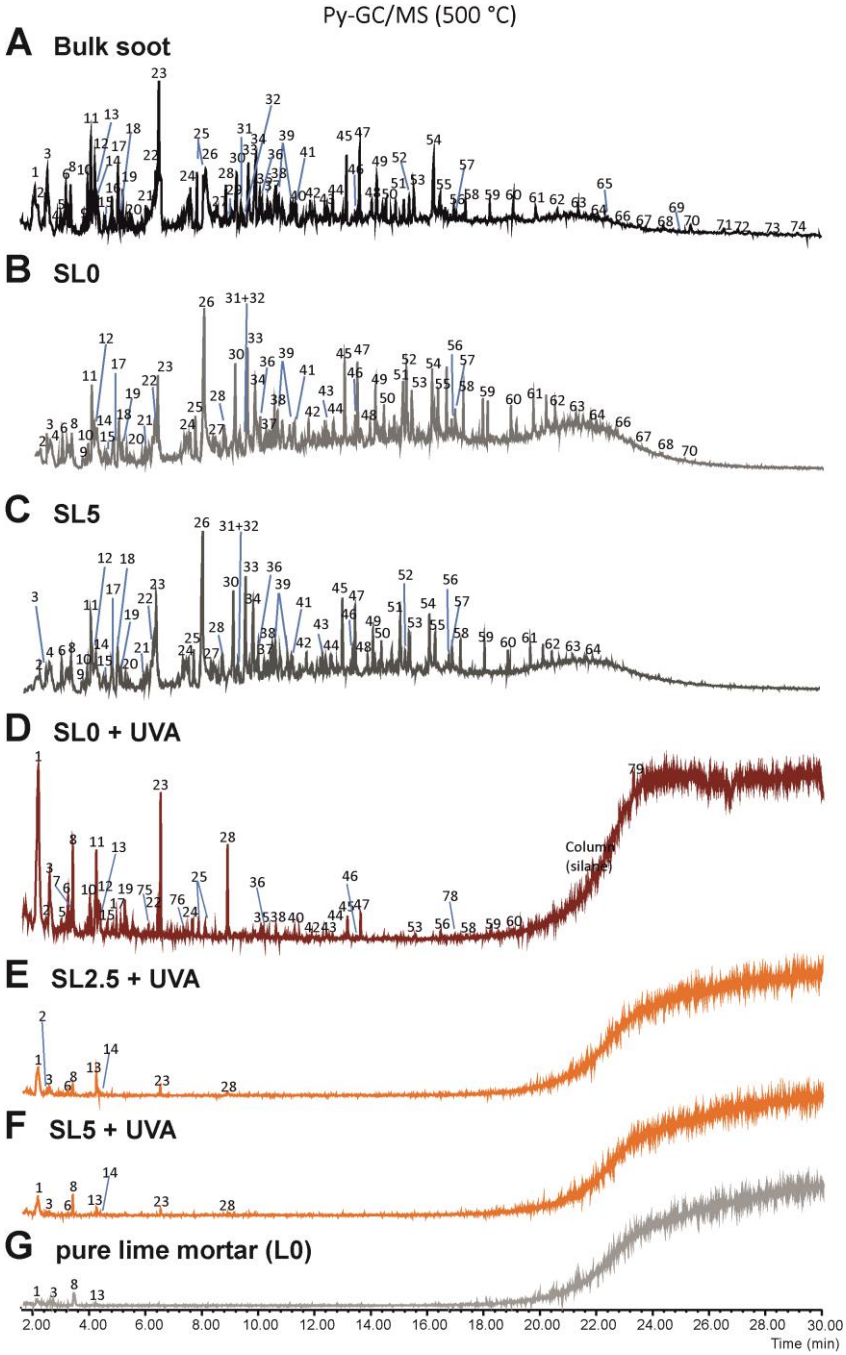

Figure 5. Total Ion Chromatograms (TIC) obtained by flash pyrolysis at 500 ºC of: A) bulk soot; B) soot-coated mortar with 0% TiO_2 before UVA irradiation (SL0); C) soot-coated mortar with 5% TiO_2 before UVA irradiation (SL5); D) soot-coated mortar with 0% TiO_2 after UVA irradiation (SL0+UVA); E) soot-coated mortar with 2.5% TiO_2 after UVA irradiation (SL2.5+UVA); F) soot-coated mortar with 5% TiO_2 after UVA irradiation (SL5+UVA), and G) pure lime mortar material (L0). Peak labels correspond to compounds listed in Table 3.

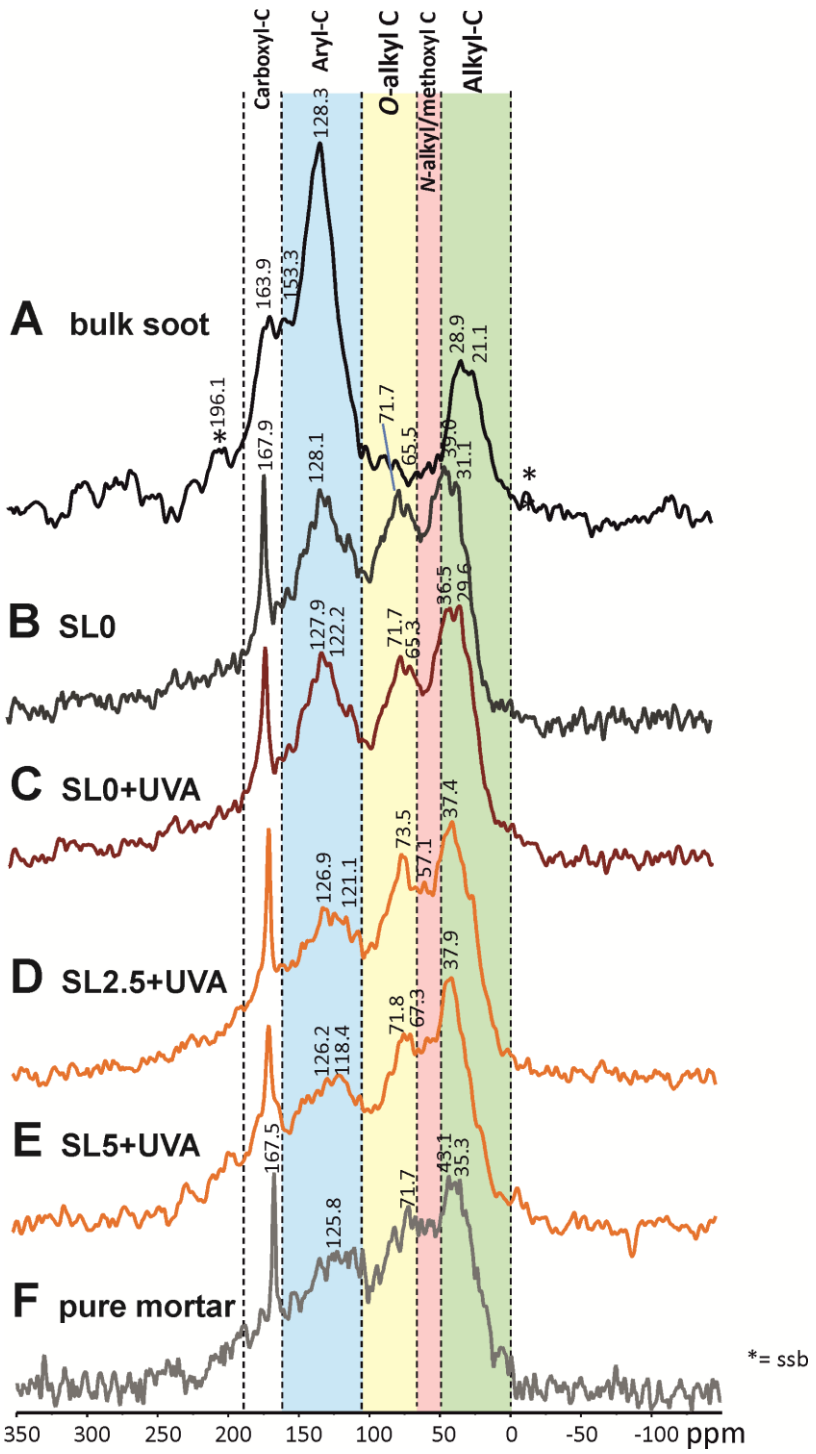

Figure 6. Solid-state ^{13}C NMR spectra of: A) bulk soot; B) soot-coated mortar with 0% TiO_2 before UVA irradiation (SL0); C) soot-coated mortar with 0% TiO_2 after UVA irradiation (SL0+UVA); D) soot-coated mortar with 2.5% TiO_2 after UVA irradiation (SL2.5+UVA); E) soot-coated mortar with 5% TiO_2 after UVA irradiation (SL5+UVA), and F) pure lime mortar material (L0).